Magnetic Resonance Imaging, Vol. 2, pp. 23–32, 1984
Printed in the USA.

0730-725X/84 $3.00 + .00

• *Research Article*

CONTRAST MANIPULATION IN NMR IMAGING

W. H. PERMAN,* S. K. HILAL, H. E. SIMON AND A. A. MAUDSLEY
Neurological Institute, Department of Radiology, Columbia-Presbyterian Medical Center, New York, NY 10032

The past few years have shown rapid growth of NMR imaging in both image quality and diagnostic usefulness. It has become apparent, as the images have been published, that both inter- and intra-group imaging of the same underlying pathology produces images which can have vastly differing appearance. This effect is mainly due to imaging techniques which use different pulse sequence types and timings thus varying the relative contribution of the protpn density, T_1, and T_2 properties of the tissues. In this paper we investigate the contrast manipulation effects and methods for SNR optimization for the saturation recovery, inversion recovery, spin echo, and inversion recovery spin echo pulse sequences when applied to three clinically relevant imaging tasks.

Keywords: **NMR, Imaging, Contrast manipulation, Signal-to-noise ratio.**

INTRODUCTION

The past few years have shown rapid growth of NMR imaging in both image quality and diagnostic usefulness. It has become apparent, as the images have been published, that both inter- and intra-group imaging of the same underlying pathology produces images which can have vastly differing appearances. While hardware factors such as rf and receiver coil inhomogeneity, as well as improperly set 90 and 180 degree pulses, contribute to these differences, the effect is mainly due to imaging techniques which use different pulse sequence types and timings.

While others have shown the qualitative effects of using different pulse sequences, there has not been a rigorous comparison of the different pulse sequences for the same imaging task on the same NMR imaging system or a rigorous investigation of the best pulse sequence timing to use for a given clinical problem. The purpose of this paper is to quantitatively investigate the contrast manipulation effects of four different pulse sequences and different timings for the same pulse sequence.

BACKGROUND

In order to understand the contrast manipulation effects of the pulse sequences we must first develop the relationship between image voxel intensity, I, and the relaxation times, T_1 and T_2, which, together with the net aligned proton density, M_0, determine the available induced voltage for a given pulse sequence.

The saturation recovery pulse sequence is illustrated in Figure 1a. A 90° rf pulse rotates the net aligned spin magnetization, $\dot{M}_z$, into the x-y plane; the resulting transverse magnetization precesses causing a free induction decay (FID) of that *rf* signal which induces a "Faraday Law" emf in the receiver coil. Due to magnet inhomogeneity the ovserved direct FID decays at a faster rate than the ideal FID, with a field-inhomogeneity decay time (T_2^*) which is shorter than the actual T_2. The initial amplitude of the FID is proportional to the $\hat{z}$ component of the net aligned magnetization at the time when the 90° rf pulse was applied. After a time τ_r, we repeat the sequence and collect the next set of data which can be at either the same angle/phase encoding for signal averaging, or a new angle/phase encoding, thereby continuing the imaging process. Quantitatively, the recovery of the aligned magnitization along the $\hat{z}$ axis due to longitudinal relaxation (T_1) is modeled by the Block equations (1) where $M_x = M_y = 0$, at $t = 0$,

$$d\dot{M}_z/dt = -(\dot{M}_z - \dot{M}_o)/T_1. \quad (1)$$

If we integrate this equation with $\dot{M}_z = \dot{M}_o$ at $t = \infty$ we find

$$\dot{M}_z = \dot{M}_o(1 - \exp(-\tau_r/T_1)), \quad (2)$$

RECEIVED 7/6/83; ACCEPTED 7/21/83.
Supported by NIH Grant No. CA-28881.

*Currently at: Dept. of Medical Physics, Univ. of Wisconsin-Madison, Madison, Wisconsin 53706.

where τ_r is the reptition time of the pulse sequence. The image voxel intensity for a linear stationary system will then be given by

$$I = K\dot{M}_z = \dot{M}'_o(1 - \exp(-\tau_r/T_1)), \quad (3)$$

where $\dot{M}'_o = K\dot{M}_o$ is the effective net equilibrium value of magnetization available for detection, accounting for system specific parameters such as coil efficiency. The important point is that for a given system K will be a constant whose value will vary only when a major system hardware change is made, such as receiver coil, rf amplifier, or receiver preamplifier.

The inversion-recovery $180 - \tau_d - 90 - \tau_r$ pulse sequence (IR-SR) is illustrated in Figure 1b. In this sequence the net aligned spin magnetization is first inverted by means of a 180° pulse, then allowed to recover due to T_1 relaxation for a time τ_d when a 90° pulse is applied, rotating the available magnetization ($\dot{M}_z$) into the $\hat{x}$-$\hat{y}$ plane for detection. An FID signal is recorded whose initial height is proportional to $\dot{M}_z$ at the time when the 90° pulse was applied. Solving the Bloch equations for the boundary conditions of $\dot{M}_x = \dot{M}_y = 0$ at $t = 0$, and $\dot{M}_z = -\dot{M}_z$ at $t = \tau_r$ yields

$$\dot{M}_z = \dot{M}_o[1 - 2\exp(-\tau_d/T_1) + \exp(-\tau_r/T_1)], \quad (4)$$

therefore,

$$I = \dot{M}'_o[1 - 2\exp(-\tau_d/T_1) + \exp(-\tau_r/T_1)]. \quad (5)$$

The 90-τ-180 spin-echo sequence is shown in Figure 1c. In this sequence a 90° rf pulse applied along the x axis rotates the net spin magnetization into the $\hat{x}$-$\hat{y}$ plane along the $\hat{y}$ axis. A time "τ" later, a 180° pulse is applied along the $\hat{y}$ axis which causes all the dephasing

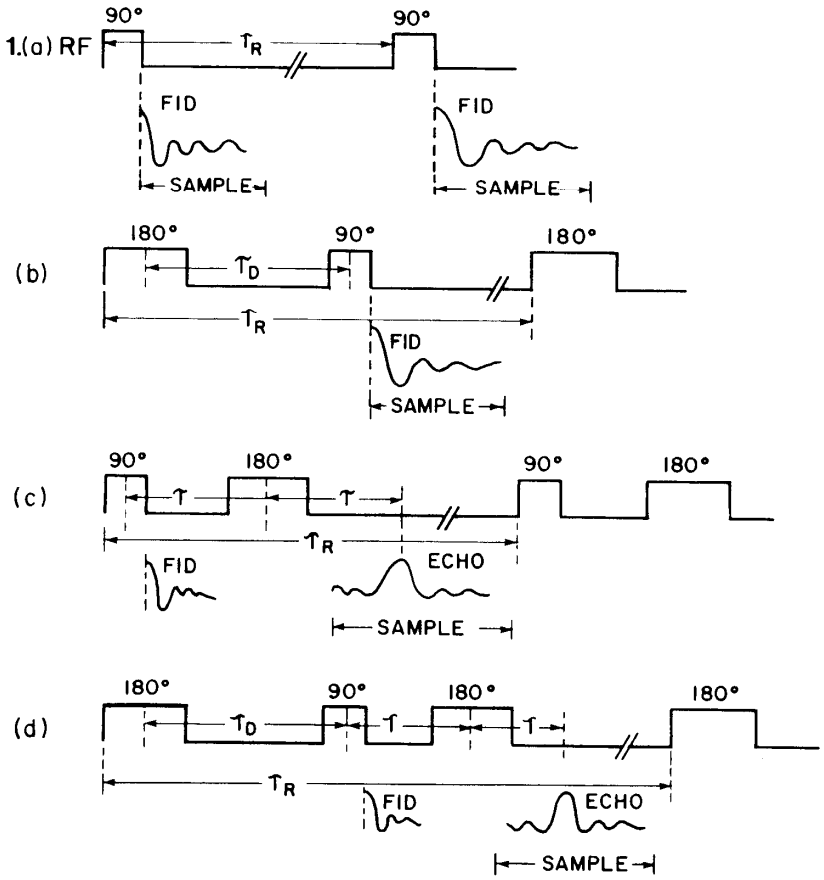

Fig. 1. The four basic pulse sequences are (a) saturation recovery (SR) where a time τ_R seperates repetitive 90° rf pulses; (b) inversion-recovery partial saturation (IR-SR) where the spins are inverted with a 180° rf pulse then a time τ_D later they are rotated into the x-y plane for detection by a 90° rf pulse; (c) spin echo (SE) sequence where a 90° rf pulse rotates the net magnetization into the x-y plane, then a time τ later a 180° rf pulse is applied which causes the free induction decay (FID) to reform as an echo of reduced amplitude due to T_2 decay at a time equal to 2; (d) inversion-recovery spin echo (IR-SE) where the net magnetization is first inverted using a 180° rf pulse before the spin echo sequence is applied.

spin isochromats to rotate 180° about the $\hat{y}$ axis. In this manner, spin isochromats which, due to field inhomogeneity, were dephasing faster than the Lamour frequency are transposed in phase so that they now follow those spin isochromats which were dephasing slower than the Lamour frequency. The net result is that after a time τ, all spins regain phase coherence along the $\hat{y}$ axis inducing an "echo" pattern in the receiver coil. The amplitude of the echo at time 2τ is then determined by the transverse relaxation (T_2), thus solving the Bloch equations for this sequence we find

$$I = \dot{M}_o' [\exp(-2\tau/T_2)] [1 - 2\exp(-\tau_d/T_1) + \exp(-\tau_r/T_1)]. \quad (6)$$

We are now in a position where, given the T_1 and T_2 values of two tissues, we can calculate the relative imaged voxel intensity for all four of the above pulse sequences.

EXPERIMENTAL RESULTS AND DISCUSSION

First, let us examine the effect of the pulse sequence type and timing on the soft tissue discrimination of gray-white matter in the brain. In Figure 2a we plot relative signal vs repetition time for both gray (T_1 = 500, T_2 = 80 msec) and white (T_1 = 250, T_2 = 40 msec) matter.[2] Here we have set $(\dot{M}_o)_{\text{white}} = (\dot{M}_o)_{\text{gray}} = 1.0$ based upon the data of Gore *et al.*[3] and the proton density images of Bydder *et al.*[2] which show little or no contrast between gray and white matter in the brain.

Note that for short repetition times both gray and white matter have relatively weak signals and the difference between them is small. At long repetition times ($\tau_r > T_1$), both tissues have relaxed almost to the equilibrium value; again the difference between the two signals is small. An expression which considers both the intensity difference between voxels and the relative magnitude of the voxels as compared to the background noise is called the signal-to-noise ratio. In our units, $I \cdot \{\text{voxel volume}\}$ is the FID signal level contributed by a single resolvable volume, and King's[4] general expression for image signal-to-noise ratio can be written in the form

$$\text{SNR} = \frac{I \cdot \{\text{voxel volume}\}\{m_v N\}^{1/2}}{\{\text{noise variance}\}^{1/2}}. \quad (7)$$

In Eq. 7, m_v is the number of resolvable voxels in the subject scan, N is the number of averages of the same cycle for noise reduction, and {noise variance} is the system FID noise variance measured in a sampling bandwidth $\{1/T_2^*\}$. This shows that, when intercomparing images obtained with different pulse sequences and/or timings on the same NMR system, the NMR image noise is a constant. It is independent of the pulse sequence and depends only upon the sampling time and the number of FID's averaged. Further, we assume the imaging system is linear such that a voltage on the projection is linearly and reproduceably mapped into an image voxel whose intensity is then proportional to the sum of all emf's received by the coil from that voxel of tissue. Using these assumptions we derive the SNR for an image voxel formed by projections of noise variance σ_p^2 given by

$$\text{SNR} = K(I_a - I_b)\sqrt{N} / \sigma_p \quad (8)$$

where K contains the geometrical and algorithmic constants. Note that this definition of SNR differs

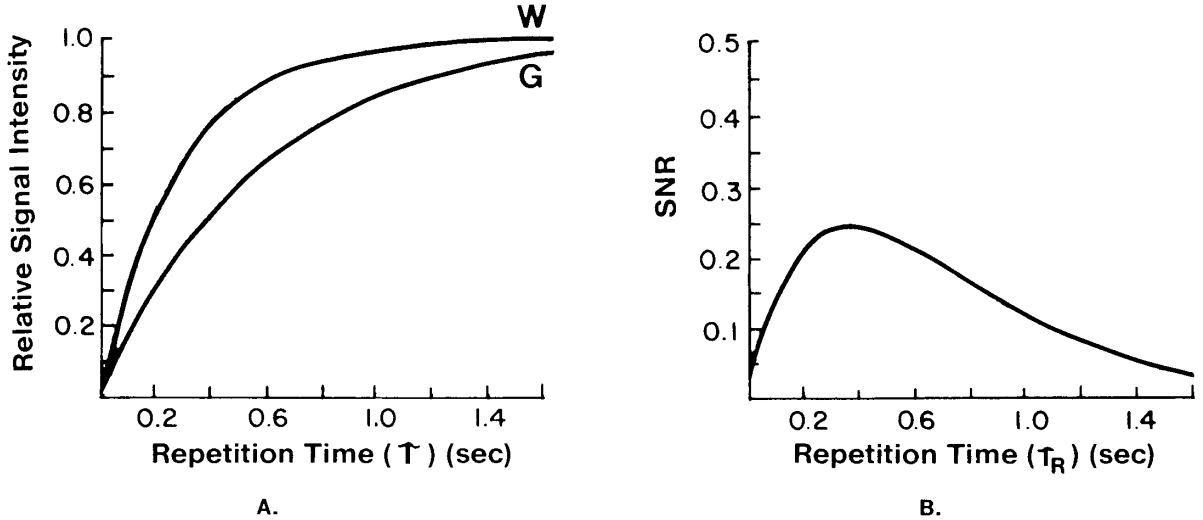

Fig. 2. The relative signal intensity for gray-white matter contrast calculated using equation 3 is plotted as a function of repetition time, τ_R (a). The SNR obtained using equation 8 is plotted as a function of τ_R in (b).

from that of Mansfield[5] and Edelstein[6] in that we have not normalized our SNR to constant scan time by including $\sqrt{\tau_r}$ in the numerator of Eq. 8. While the general form of a SNR for constant scan time is valid, we believe that for slice-oriented imaging the physician will need more than one slice in order to make a diagnosis. This requirement leads us to multi-slice imaging where the desire for short scan times is offset by the need to keep the repetition time long compared with the data collection time (i.e. $\tau_r \gg \tau_{data}$). That is, if we use $\tau_r = T_1 = 800$ msec and $\tau_{data} = 80$ msec, we can do 10 multi-slice data collections in a single repetition time. However, if we decrease τ_r to 150 msec and increase N to 7 we do get a large SNR advantage (Figure 7a), but now we can only image one slice due to the short τ_r time. Therefore, in the simulations that follow we assume that multi-slice imaging will be essential for clinical NMR,[7] and we set $\sqrt{N} = 1$ in Eq. 8 as this N must be used to collect additional slices instead of decreasing the image noise through signal averaging.

In Figure 2b we plot the relative SNR vs repetition time for gray and white matter. The curve exhibits a broad maximum at $\tau_r = 360$ msec. This result where $\tau_r(\max) = \{(T_1)_g + (T_1)_w\}/2$ agrees with predictions by others[8,9,10] and serves as a basis for the comparisons which follow.

The calculations for the 180-τ_d-90 inversion recovery sequence (IR-SR) for imaging gray and white matter are shown in Figure 3. We plot the relative signal vs τ_d for successively shorter repetition times in Figures 3a–c. Note that for long τ_r (Figure 3a), I_w is greater than I_g since $(T_1)_w$ is less than $(T_1)_g$ and both tissues have been allowed sufficient relaxation time to reach their equilibrium values. As τ_r approaches the tissue T_1's, we find a point where the difference in signals is zero, i.e. a crossover region where $I_g > I_w$ on the left and $I_g < I_w$ on the right. The reason for this anomaly is that the tissue with the shorter T_1 relaxes towards equilibrium faster producing a more negative signal upon inversion. After the inversion pulse the short T_1 tissue relaxes at a faster rate so that its relaxation curve crosses that of the longer T_1 tissue. The importance of this crossover point is shown in Figure 3d where we plot the relative SNR vs τ_d. When τ_r is long compared to the respective tissue T_1's, the

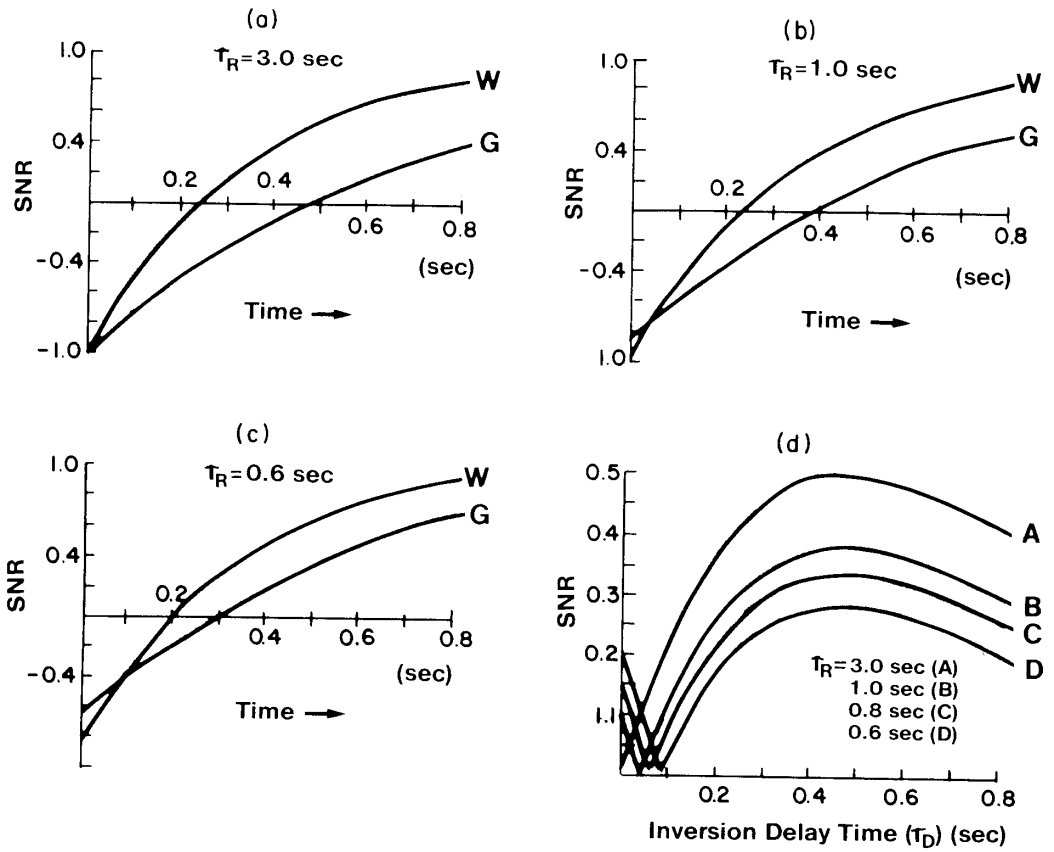

Fig. 3. The relative signal intensity vs inversion delay time, τ_D, for IR-SR sequence applied to imaging gray-white matter is plotted for repetition times of (a) 3.0 sec, (b) 1.0 sec, and (c) 0.6 sec. The SNR vs τ_D for the IR-SR sequence is plotted in (d) for four repetition times. Note the crossover region for repetition times B-D.

curve exhibits constant positive contrast (white matter brighter than gray matter) with a broad maximum at $\tau_d = 400$ msec. When τ_r is on the order of the tissue T_1's, the SNR curve has a crossover point with negative contrast to the left ($I_g \gg I_w$) and positive contrast to the right ($I_g < I_w$). In addition, the negative contrast region has increasing SNR with decreasing τ_r, whereas the positive contrast region has the expected decreasing SNR behavior with decreasing repetition time. Therefore if we are operating to the left of the crossover point we maximize the relative SNR by decreasing both τ_d and τ_r. If we are operating to the right of the crossover point the relative SNR has a maximim at $\tau_d = 400$ msec, the position of the maximum remaining constant as the relative magnitude decreases due to decreasing repetition time.

The gray-white matter calculations for the 90-τ-180 spin echo (SE) sequence are shown in Figure 4. We plot the relative signal intensity vs spin echo time τ for three different repetition times in Figures 4a–c. Note again the interesting feature of a crossover point as the repetition time approaches 1 sec. If we examine Eq. 6 we find the spin echo intensity is given by a T_2 dependent factor multiplying a T_1 dependent factor. As in the SR and IR-SR cases shown above, the crossover effect is due to the rapid recovery of the T_1 dependent factor modulated in spin echo imaging by the T_2 factor. Note that as τ_r becomes short, the crossover point shifts toward longer spin echo times. In Figure 4d we plot the relative SNR vs τ for several repetition times. The negative contrast region behaves as above with increasing SNR resulting from shorter spin echo times and decreasing repetition times. The positive contrast region differs from the above case in that as τ_r decreases, not only does the crossover point shift dramatically toward longer (normally used) spin echo times, but also the maximum SNR value shifts toward longer spin echo times.

The effect of using an inversion 180-τ_d-90-τ-180 spin echo (IR-SE) sequence to discriminate between gray and white matter is shown in Figure 5. The plots of relative signal intensity vs τ_d for constant $\tau = 30$ msec show a crossover point which occurs at significantly longer τ_d times; this same point shifts inward toward shorter τ_d for decreasing τ_r. This behavior is due to the exp $(-\tau_r/T_1)$ term in Eq. 6; now both tissues are not relaxing toward the same dynamic equilibrium as dictated by the repetition time. When plotting the

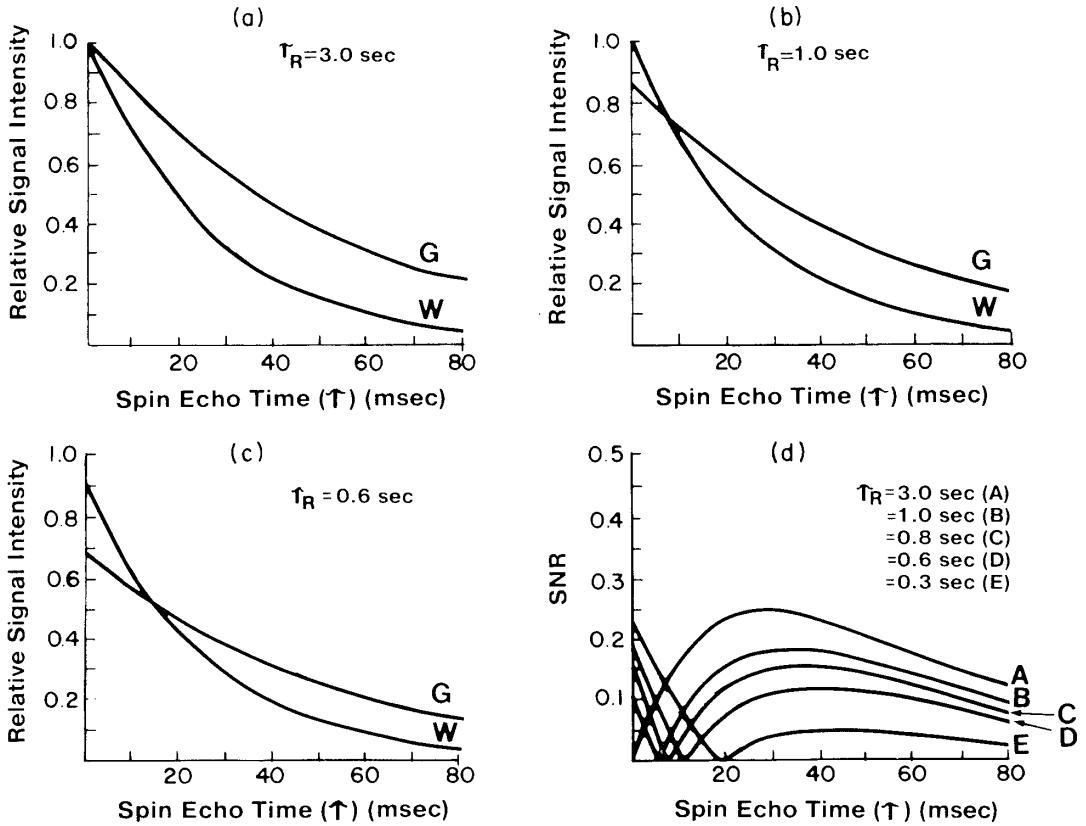

Fig. 4. The relative signal intensity vs spin echo time, τ, for the SE sequence as applied to gray-white matter contrast for repetition times (a) 3.0 sec, (b) 1.0 sec, (c) 0.6 sec. The SNR vs τ for the SE sequence is plotted in (d) for four repetition times. Again, note the crossover regions for repetition times B–E.

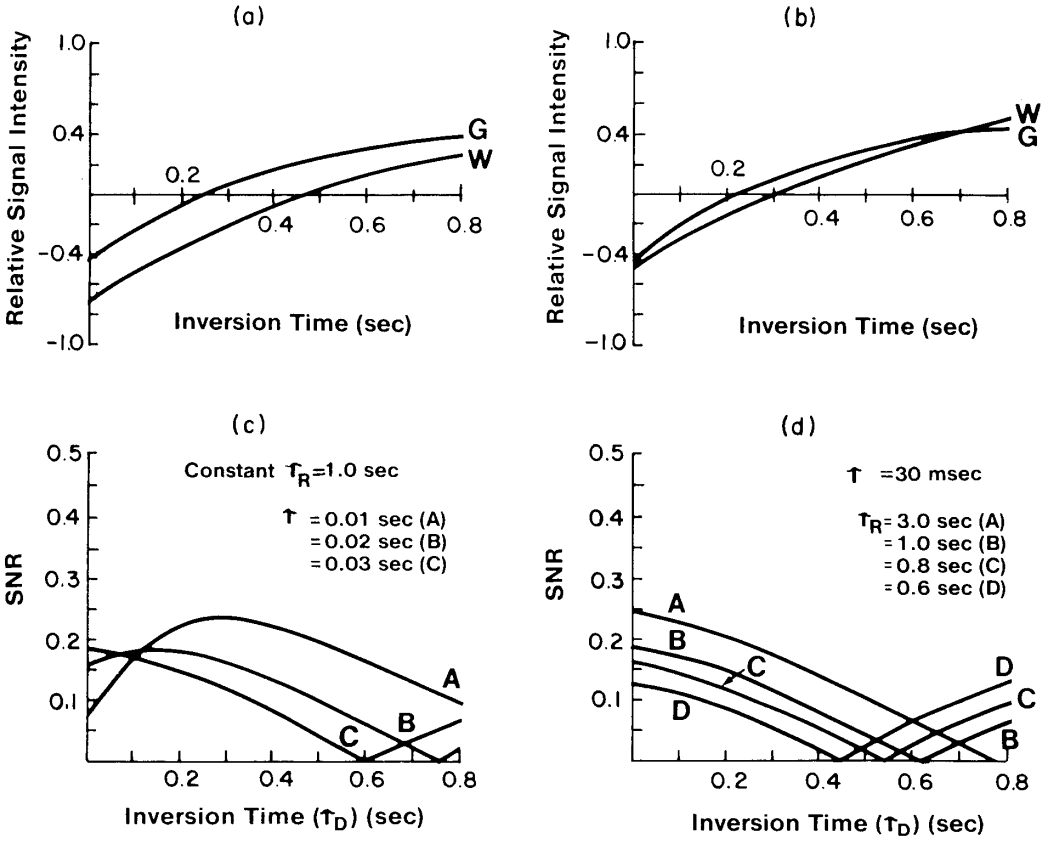

Fig. 5. The relative signal intensity vs τ_D for gray-white matter contrast using the IR-SE sequence is plotted for repetition times of (a) 3.0 sec, and (b) 0.6 sec. The SNR vs τ_D for the IR-SE sequence is plotted for three spin echo times at constant repetition times (c), and for three repetition times at constant spin echo time (d). Again, note the crossover regions in (c) and (d).

SNR vs τ_d for the spin echo sequence we must consider the effect of varying both the repetition time and the spin echo time on the predicted SNR. In Figure 5c we plot SNR vs τ_d for constant τ_r = 1 sec while varying the spin echo time τ. Note that as the spin echo time increases, the maximum SNR magnitude decreases and shifts toward shorter τ_d times. When τ is on the order of the tissue T_2's (τ = 30 msec) the maximum SNR value occurs at τ_d = 0 msec, indicating the strong influence of the tissue T_2's upon this imaging sequence. If we hold τ constant at 30 msec and vary τ_r (Figure 5d), we find that the maximum SNR value occurs at τ_d = 0 msec for all τ_r, with the relative magnitude decreasing with decreasing τ_r. It is interesting to note that unlike the IR-SR case, where the optimal τ_d value is 400 msec, the optimal value for the IR-SE case occurs at a much shorter τ_d time of 120 msec for τ = 20 msec.

For comparison purposes we have replotted the SNR curves of all four pulse sequences as applied to the discrimination of gray and white matter in Figure 6. The maximum SNR for this clinical task is obtained using the IR-SR pulse sequence with τ_d = 400 msec. However, if we normalize our SNR to constant time by plotting SNR/$\sqrt{\tau}$ vs τ_r (Figure 7), we find the maximum SNR is obtained using the SR sequence with a repetition time of 150 msec. Note that while the IR-SR sequence is almost as efficient, both spin echo sequences suffer from decreased signal because T_2 modulation decreases both SNR's by almost a factor of two.

Another clinically interesting application is the detection of an infarct in surrounding brain tissue. The typical presentation of an infarct in NMR is a loss of gray and white matter contrast, and a T_1 value longer than that of gray matter.[2] Also Crooks *et al.*[11] have shown that there is an increase in the T_2 value of the infarcted tissue with respect to normal brain tissue (both gray and white matter). We have modeled an infarct region having a T_1 = 800 msec, and a T_2 = 200 msec. The results for infarct vs white matter are plotted in Figure 8, and for infarct vs gray matter in Figure 9. The SNR curves for infarct vs white matter are similar to those for gray and white matter contrast, with the optimal IR-SR τ_d time shifting to a longer value of 550 msec. However, the infarct vs gray matter

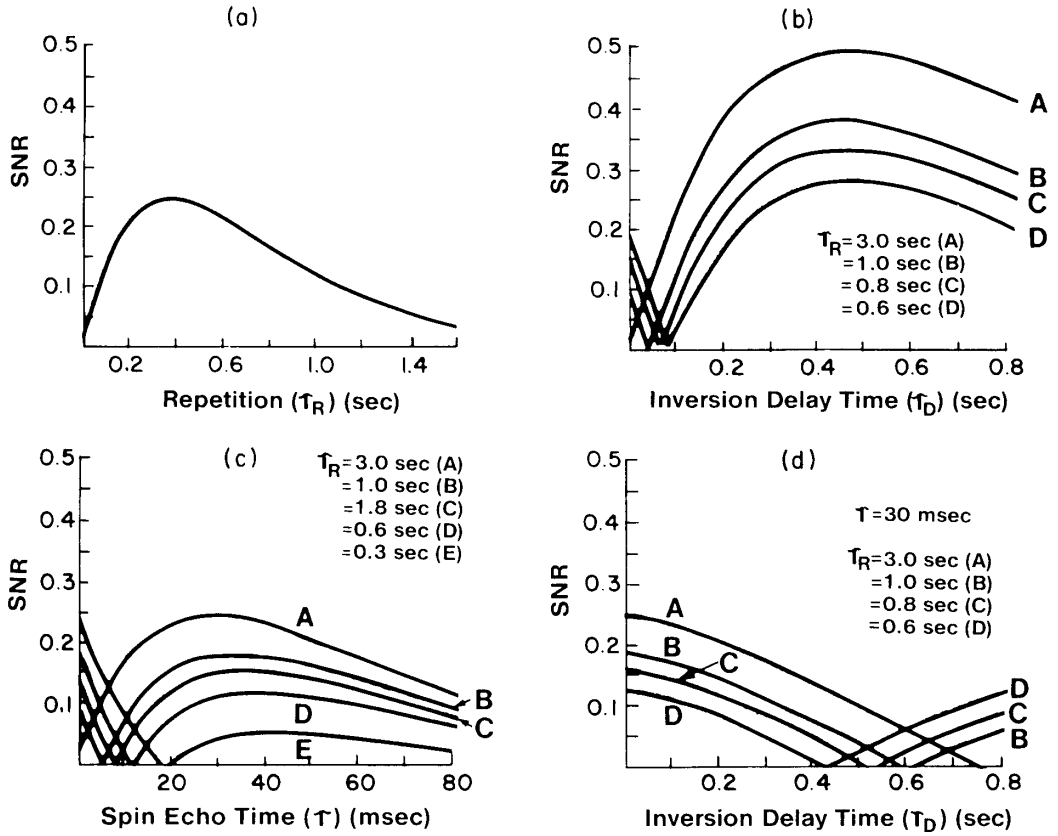

Fig. 6. Summary of SNR behavior calculated for gray-white matter contrast for (a) SR, (b) IR-SR, (c) SE, and (d) IR-SE.

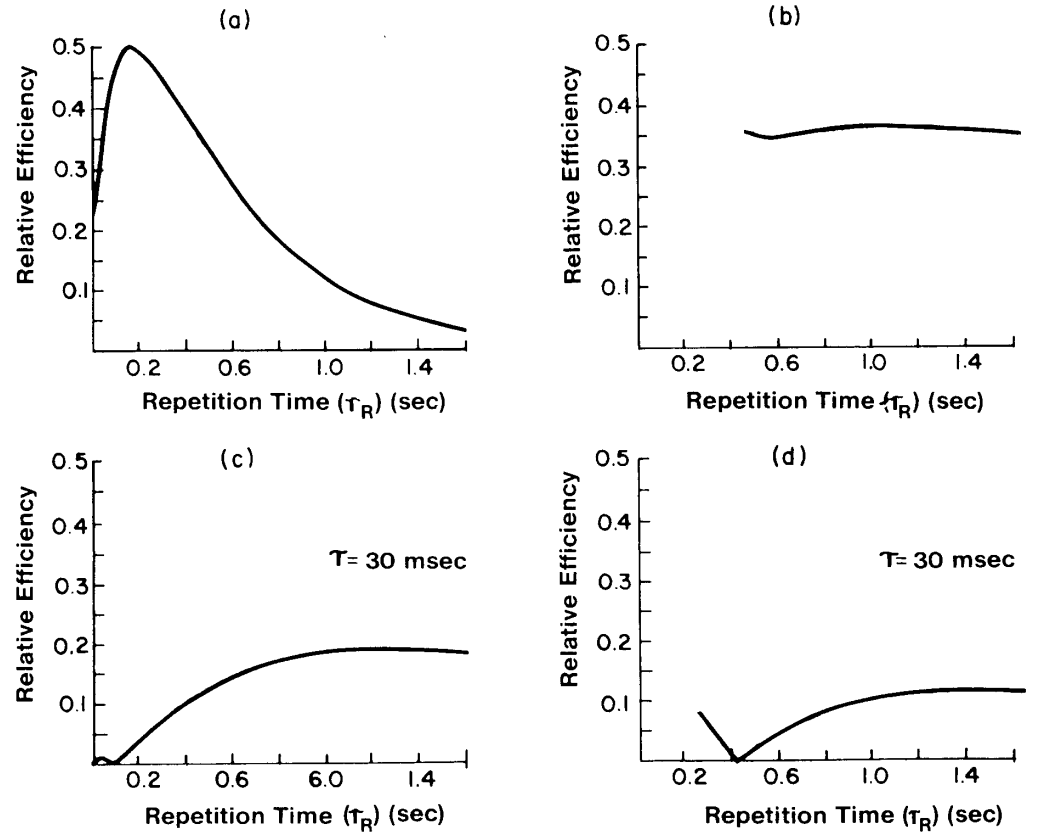

Fig. 7. The SNR per unit imaging time (relative efficiency SNR/$\sqrt{\tau_R}$) is plotted vs τ_R for (a) SR, (b) IR-SR, (c) SE, (d) IR-SE.

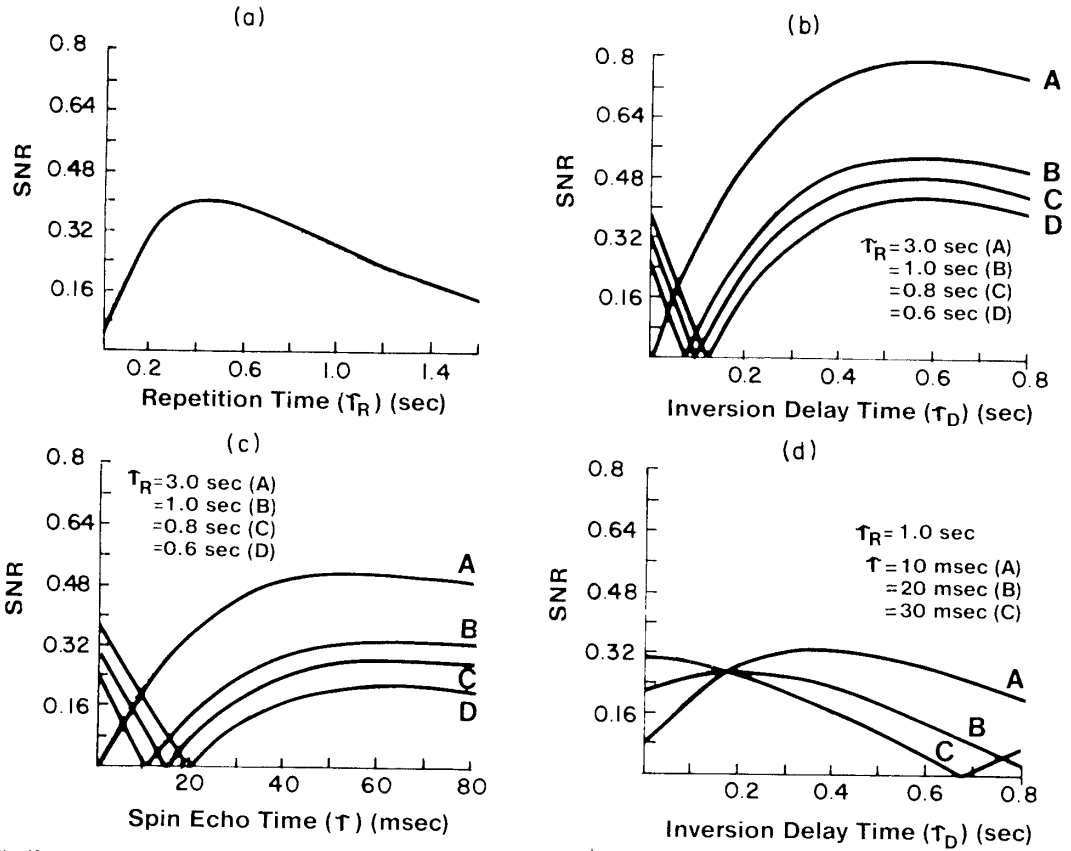

Fig. 8. Summary of SNR behavior calculated for an infarct vs white matter contrast using (a) SR, (b) IR-SR, (c) SE, and (d) IR-SE.

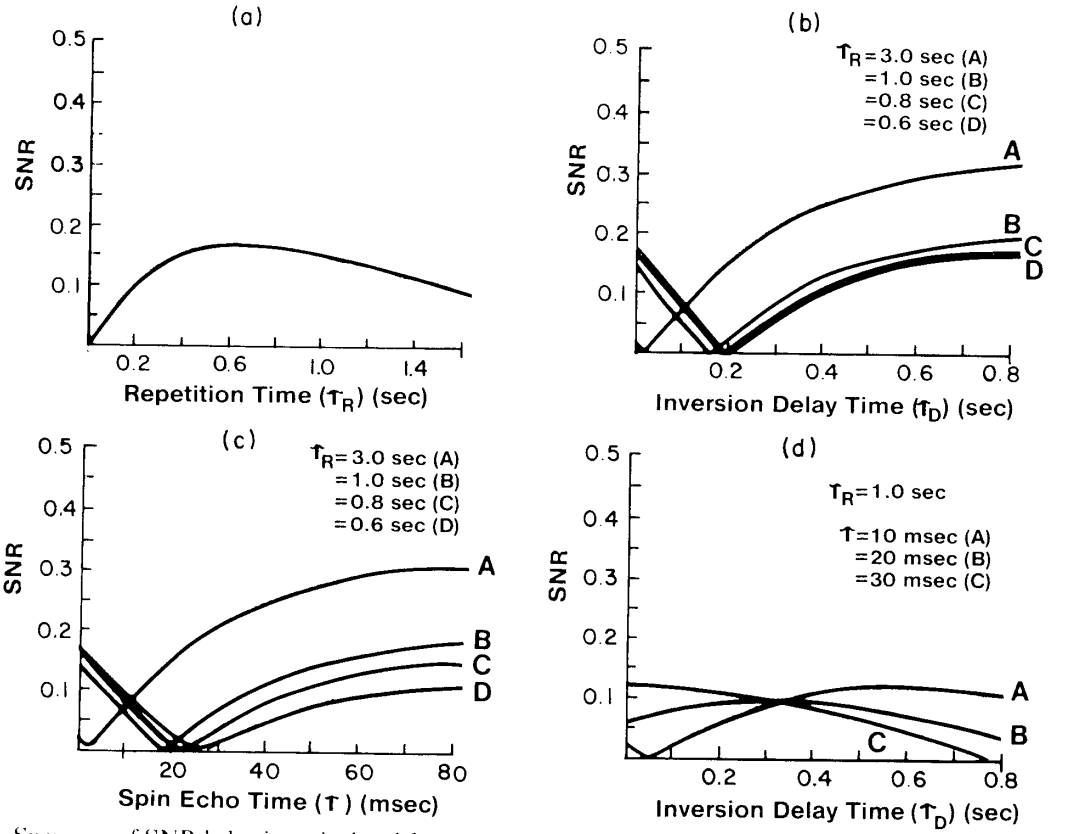

Fig. 9. Summary of SNR behavior calculated for an infarct vs gray matter contrast using (a) SR, (b) IR-SR, (c) SE, and (d) IR-SE.

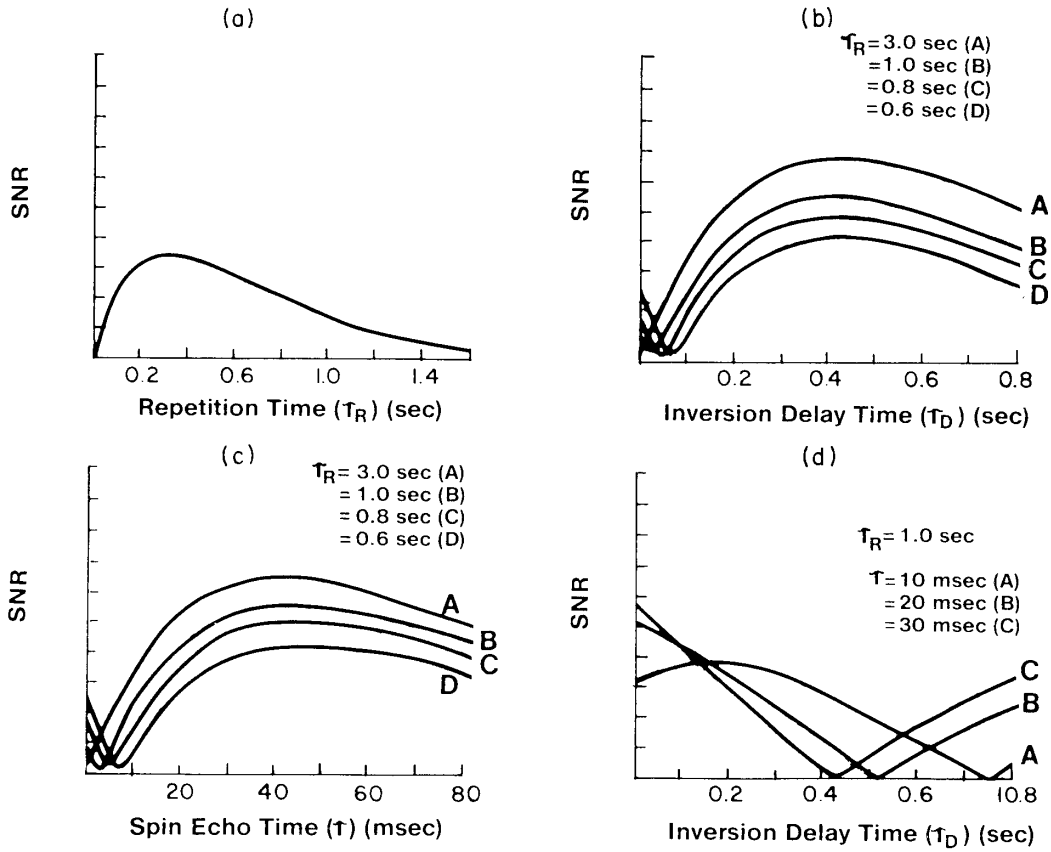

Fig. 10. Summary of SNR behavior calculated for demylinization vs white matter using (a) SR, (b) IR-SR, (c) SE, and (d) IR-SE.

curves show steadily increasing signal as τ_d increases, with all four pulse sequences having approximately equal sensitivity. This is due to the loss of T_1 signal as ΔT_1 (infarct-gray) is less than ΔT_1 (gray-white) for the SR and IR-SR sequences, and to the increase in T_2 signal as ΔT_2 (infarct-gray) is greater than ΔT_2 (gray-white) for the SE and IR-SE sequences.

Finally let us examine the clinical task of diagnosing and monitoring demyelinating dideases such as multiple sclerosis and Huntington's chorea. In general, a demyelinating plaque will have a T_1 value which is less than that of gray matter but larger than that of white matter, and a T_2 value which is longer than the T_2 value of gray matter but shorter than that of cerebrospinal fluid.[2] In Figure 10 we model demyelination vs white matter for plaques having T_1 = 400 msec and T_2 = 100 msec. The resulting SR and IR-SR curves are similar to those for gray and white matter, but the SE and IR-SE curves are significantly different. The SE curves now show a SNR magnitude equivalent to those of IR-SE with the crossover point shifting toward shorter (less useful) spin echo times. The IR-SE plots exhibit crossover points at short τ_d times, and the maximum signal occurs at τ_d = 0, i.e. spin echo sequence without the inversion.

CONCLUSIONS

The purpose of this paper has been to show the underlying physical basis for contrast manipulation and optimization in NMR imaging. In CT and other diagnostic X-ray imaging modalities the image contrast is manipulated by changing the kVp of the X-ray source, in NMR the image contrast is manipulated by varying the relative contributions of the T_1 and T_2 factors by changing the type of pulse sequence and the timing parameters of the sequence. In the simulations above we have tried to use accurate T_1 and T_2 values for the tissues, but they are not well defined in the literature and are subject to variation with a change in the static field strength. Therefore while the above simulations are quantitative in terms of the imaging parameters selected, the reader should use the results as templates for understanding the physical properties of his imaging application when selecting the appropriate pulse sequence and timing parameters.

While the methods employed in radiological imaging to maximize the image SNR are straightforward, we find the anomaly of a "crossover" region in NMR imaging. It becomes imperative to know which side of the crossover region we are operating on as the rules for

maximizing the SNR are diametrically opposed for the two regions. In general if we are to the left of the crossover point, the SNR is maximized by decreasing the repetition time and shortening the inversion time; if we are operating to the right of the crossover point the repetition and inversion times should be lengthened.

The situation for spin echo imaging is even more complex because the spin echo time τ is dictated by the magnet inhomogeneity and sampling constraints for a given image resolution. For example, an inhomogeneous magnet will have a short T_2^* allowing the choice of a short τ; the sensitivity, however, is decreased due to the larger imaging gradients needed to obtain the same spatial resolution as that of a magnet having better homogeneity; the latter's longer T_2^* requires the selection of a longer τ. Although the spin echo sequence does not provide equivalent SNR for lesions having a large T_1 contrast, clinical results[11] indicate that the T_2 contrast is useful in differentiating tumors from edema. The ramifications of the crossover regions in the above simulations are serious for clinical applications. Care must be taken when selecting pulse sequence and timing parameters because, unlike the situation with X-ray CT, it is possible to manipulate the T_1 and T_2 factors so that all image contrast is lost. Furthermore, since at this time the range in values of T_1 and T_2 for a given lesion are not known, at least two imaging sequences per slice will be necessary to guarantee that a lesion has not been overlooked.

In conclusion, our simulations indicate that, due to the complex nature of image contrast in NMR imaging, there will not be a universal pulse sequence which maximizes the SNR for all imaging applications. Instead we feel that, as the T_1 and T_2 values of different lesions are defined, pulse sequence protocols will evolve which are best able to maximize the SNR and answer the clinical questions.

REFERENCES

1. Farrar, T.C.; Becker, E.D. *Pulse and Fourier Transform NMR*. New York: Academic Press, 1971.
2. Bydder, G.M.; Steiner, R.E.; Young, I.R.; Hall, A.S.; Thomas, D.J.; Marshall, J.; Pallis, C.A.; Leff, N.J. Clinical NMR imaging of the brain: 140 cases. *Amer. J. Radiol.* 139:215–236; 1982.
3. Gore, J.C.; Doyle, F.H.; Pennock, J.M. Nuclear magnetic resonance (NMR) imaging at Hammersmith Hospital. *SPIE* 273:8–10; *Application of Optical Instr. in Medicine* IX, 1981.
4. King, K. Signal-to-noise ratios in NMR imaging. Ph.D. thesis, Univ. Wisconsin-Madison 1982; available from Univ. Microfilms, Ann Arbor, Michigan; also available from Univ. Wisconsin-Madison as technical report WMP-166.
5. Mansfield, P.; Morris, P.G. *NMR Imaging in Biomedicine*. New York: Academic Press, 1982.
6. Edelstein, W.A.; Bottomley, P.A.; Hart, H.R.; Smith, L.S. Signal, noise, and contrast in nuclear magnetic resonance (NMR) imaging. *J. Comput. Assist. Tomogr.* 7:391–401; 1983.
7. Crooks, L.E.; Ortendahl, D.A.; Kaufman, L.; Hoenninger, J.; Arakawa, M.; Watts, J.; Cannon, C.R.; Brant-Zawadzki, M.; Davis, P.L.; Margulis, A.R. Clinical efficiency of nuclear magnetic resonance imaging. *Radiol.* 146:123–128; 1983.
8. Edelstein, W.A.; Bottomley, P.A.; Hart, H.R.; Leue, W.M.; Schenck, J.F.; Redington, R.W. NMR imaging at 5.1 mHz: Work in progress. *Proc. of the Int. Symp. on Nuclear Magnetic Resonance Imaging* held at Bowman-Gray, Oct. 1–3. 1981, pp. 139–145.
9. Young, I.R.; Burl, M.; Clarke, G.J.; Hall, A.S.; Pasmore, T.; Collins, A.G.; Smith, D.T.; Orr, J.S.; Bydder, G.M.; Doyle, F.H.; Greenspan, R.H.; Steiner, R.E. Magnetic resonance properties of hydrogen: imaging the posterior fossa. *Amer. J. Radiol.* 137:895–901; 1981.
10. Young, I.R.; Bailes, D.R.; Burl, M.; Collins, A.G.; Smith, D.T.; McDonnell, M.J.; Orr, J.S.; Banks, L.M.; Bydder, G.M.; Greenspan, R.H.; Steiner, R.E. Initial clinical evaluation of a whole body nuclear magnetic resonance (NMR) tomograph. *J. Comput. Assist. Tomogr.* 6:1–9; 1982.
11. Crooks, L.E.; Mills, C.M.; Davis, P.L.; Brant-Zawadzki, M.; Hownninger, J.; Arakawa, M.; Watts, J.; Kaufman, L. Visualization of cerebral and vascular abnormalities by NMR imaging: The effects of imaging parameters on contrast. *Radiol.* 144:848–852; 1982.